FD-TD Analysis of Vivaldi Flared Horn Antennas and Arrays

Eric Thiele, *Student Member, IEEE*, and Allen Taflove, *Fellow, IEEE*

***Abstract*— This paper summarizes a detailed computational study of Vivaldi flared horn antenna designs including single element, double element, crossed-pair subarray elements, and linear arrays using the finite-difference time-domain (FD-TD) method. FD-TD, which numerically solves Maxwell's time dependent curl equations, accounts for the complex geometrical and electrical characteristics associated with this antenna design and array implementation. Validations have been made relative to a moment method (MM) model of an electrically large linearly tapered slot antenna. Also, good correlation is shown to exist in the primary features of the antenna patterns between computed and measured data for all cases.**

This work has achieved a number of *firsts* for the FD-TD methodology. It represents the first "exact" computational model of a single quad Vivaldi slot antenna; the first "exact" computational model of a phased array of Vivaldi quad elements; and the first FD-TD model to demonstrate grating lobes for a phased array antenna of any sort. Lastly, this research represents an extensive study of the largest grid-based antenna models conducted to date.

I. Introduction

SLOTLINE antennas are known to be traveling wave antennas with the capability of producing broadband, endfire radiation. A recent implementation of slotline antennas was introduced by Gibson in 1979 [1]. In this model, a microstrip slotline is flared outward to some width at which desired radiation occurs. This is referred to as a *tapered slot antenna* (TSA). It is this type of slot antenna that is under consideration in this paper.

A. Background

Derived from the slotline, the TSA is a traveling wave antenna, specifically a surface wave antenna. An advantage of this antenna over resonant antennas is its ability to work over a large bandwidth. On a fundamental level, TSA's work because fields confined in a slotline are able to decouple from the slot edges and radiate as slot width is increased. Since the structure is open ended, there is virtually no reflection of the outgoing wave, and current reflections along the edges are also small.

Analytical treatment of the TSA has not been extensive. Prasad and Mahapatra [2] develop their model by widening the slotline until radiation occurs, approximately when the slot-mode wavelength λ' becomes greater than about 0.4 λ_0. They also account for end effects in the slotline, as well as an open microstripline feed. Yngvesson *et al.* [3] examine several different slot antennas using mostly empirical design.

Janaswamy *et al.* [4], [5] present the first analytical model for linearly tapered slot antennas (LTSA). A two-step approach is taken to analyze an electrically large LTSA. In the first step, the aperture distribution is determined by breaking the tapered slot into sections ($\sim \lambda_0/5$ per section), then treating each section as an eigenvalue problem for a slotline. Matching conditions requiring power continuity are enforced between sections. In the second step, the aperture distribution is treated as an equivalent magnetic current in the presence of a half plane. An appropriate Green's function is then used to weight the distribution and obtain far-field data. Two factors limit this approach. The presence of a dielectric is accounted for only in the first step. More importantly, however, the Green's function employed assumes an infinite ground plane on either side of the aperture. The contributions from corner diffraction, which are known to be significant, are thus neglected.

The above model is able to provide a reasonable amount of correlation with measured data, as long as the front edge of the antenna is electrically large. In [6] Janaswamy acknowledges that not accounting for the finite antenna width is a significant drawback. He also states that antennas yielding narrower main beams are possible with smaller ground planes. Based on the limitations of the previous work, Janaswamy develops a more accurate moment method (MM) model capable of accounting for the finite width of the antenna. The MM approach does require some assumptions, though. An approximation to include the effects of a dielectric substrate is made through the use of a surface impedance on the MM patch elements. The geometry is also approximated to reduce the number of unknowns in the MM impedance matrix. However, the moment method procedure demonstrates much better accuracy when applied to the TSA problem than the two-step method of [5]. The results of this analysis are used as a validation of the FD-TD method.

The MM approach is also used by Simon *et al.* in [7] to determine the input impedance for a finite slot in the ground plane of a stripline. In this model the stripline conductor is replaced with an equivalent electric surface current and the slot is replaced by a perfect electric conductor where equivalent magnetic currents are defined. Thus, the total field distribution remains unchanged. The appropriate Green's functions defining the kernel of the integral equations used to fill the MM matrix are then determined in a computationally efficient manner. Triangular patch elements are then used as

Manuscript received March 10, 1993; revised September 8, 1993. This work was supported in part by Northrop Defense Systems Division, Rolling Meadows, IL, under Contract Ref. No. 1186017, and by Cray Research, Inc.

The authors are with the EECS Department, McCormick School of Engineering, Northwestern University, Evanston, IL 60208 USA.

IEEE Log Number 9401338.

the basis functions in the integral equations. This method proves to be accurate in determining the impedance of this antenna. However, an infinite ground plane is assumed, and the radiation pattern for the antenna is not obtained.

B. Approach

This paper reports a study of a stripline-fed Vivaldi TSA and then extends the analysis to an array composed of Vivaldi elements. As there are limited analytical models to study a TSA, the FD-TD model was implemented to augment existing empirical designs. FD-TD naturally accounts for the complex interactions needed to model this type of problem, such as diffraction effects due to finite ground planes, variations in phase velocities, frequency-dependent impedance, and detailed feed structures. It also allows for a straightforward calculation of far-field radiation patterns.

The primary goals were to compute the E/H plane gain patterns and input impedance across a band of frequencies from 6 GHz to 18 GHz. There were several phases to this project. The first phase consisted of examining the planar element, including both single and double flare designs. The second phase was to model the quad pair (orthogonal double flare elements). The third phase was to incorporate the quad pair element into a linear phased array.

The primary research goal during the first phase of this project was to "tune" the computational model. To that end, a baseline model was established and an extensive study was conducted of that model and the effects of minor perturbations to it. The E/H plane gain patterns were determined, and flare geometry concerns (length/rate of taper, continuous versus discrete taper) were also examined for both single and double flares. As a validation of the FD-TD method of studying this antenna type, an LTSA described in the literature was also modeled.

The more complex geometry of the quad element was computationally developed in the second phase of the project. This model consisted of two double flares made with co-location slots to allow for the mechanical assembly of the elements. This design is used to avoid entirely shorting either the horizontal or vertical ground planes. Results for E/H plane gain were determined across the bandwidth.

The final phase of this work was to incorporate the quad elements into an eight-element linear phased array. E and H plane gain patterns were computed for an equiphase array. E-plane gain patterns for beam steer angles of 20°, 45°, and 60° for selected frequencies across the bandwidth were computed for the phased array. In terms of desired research goals and the expansion of FD-TD applicability, these results constitute an important achievement for both.

II. FD-TD

In 1966, Yee [8] introduced an explicit finite differencing scheme that was able to numerically solve Maxwell's time-dependent curl equations. This work was revised and extended by Taflove and Brodwin in [9]. Further work in the areas of radiation boundary conditions (RBC's) [10], [11], computation of far field data from near field data [12], [13], and the recently introduced work of Jurgens *et al.* [14] in modeling curved surfaces has made FD-TD an attractive method for solving a number of electromagnetic interaction problems.

A. Stepped Edge FD-TD

A spatial lattice structure is used to discretize space in order to sample electric and magnetic field data. This lattice is composed of cubic cells, each containing Cartesian (x, y, and z) components of electric and magnetic fields that are interleaved in such a way so as to provide for second-order-accurate central-difference equations in space. To specify an object, the coefficients of the electric and magnetic field component update equations are set to appropriate values at each point in the cubic cell, for every cell in the FD-TD lattice. These coefficients allow for the inclusion of objects with any desired permittivities and permeabilities, as well as electric and magnetic conductivities. Electric and magnetic fields are then alternately sampled at half-time steps to give a second-order-accurate temporal central-difference equation. This results in a fully explicit set of field update equations that is second-order accurate and requires no back storage in time. This accuracy allows for the study of problems with a dynamic range of 40–50 dB [13]. A condition between space and time increments is enforced to maintain Courant stability [9].

B. Far-Field Data

For the computation of antenna patterns and radar cross section, it is necessary to have far-field data. These far-field data can be obtained from FD-TD through the powerful near to far-field transformation given in [12]. A closed surface is defined in free space that completely encloses the object modeled. Upon completion of the FD-TD algorithm, this transformation is used to define equivalent magnetic and electric surface currents based on near-field data. A surface integration of these equivalent currents, weighted by the free space Green's function, is then calculated. This integration yields two vector potentials. These potentials define the angular components of far electric fields, E_ϕ and E_θ. In terms of the computed and measured antenna patterns discussed later, E_ϕ corresponds to co-polarized electric fields (co-pol), and E_θ corresponds cross-polarized electric fields (cross-pol). Different observation angles require a recalculation of the integral.

III. Planar Vivaldi TSA and LTSA Results

The Vivaldi antenna under examination (Fig. 1) is hand-assembled from two pieces. On each, a flare is etched in copper on a dielectric substrate. On one piece, a stripline feed is etched on the other side of the substrate. These pieces are then placed together, with the feed centered between them. For measurement purposes, the feed is connected to the inner conductor of a coaxial line, with the ground planes connected to the outer conductor. This physical model forms the base element under consideration.

As we shall discuss in Section IV, the Vivaldi TSA forms the basis of an antenna array where crossed pairs of coplanar double-flare Vivaldis form the subarray elements. This array

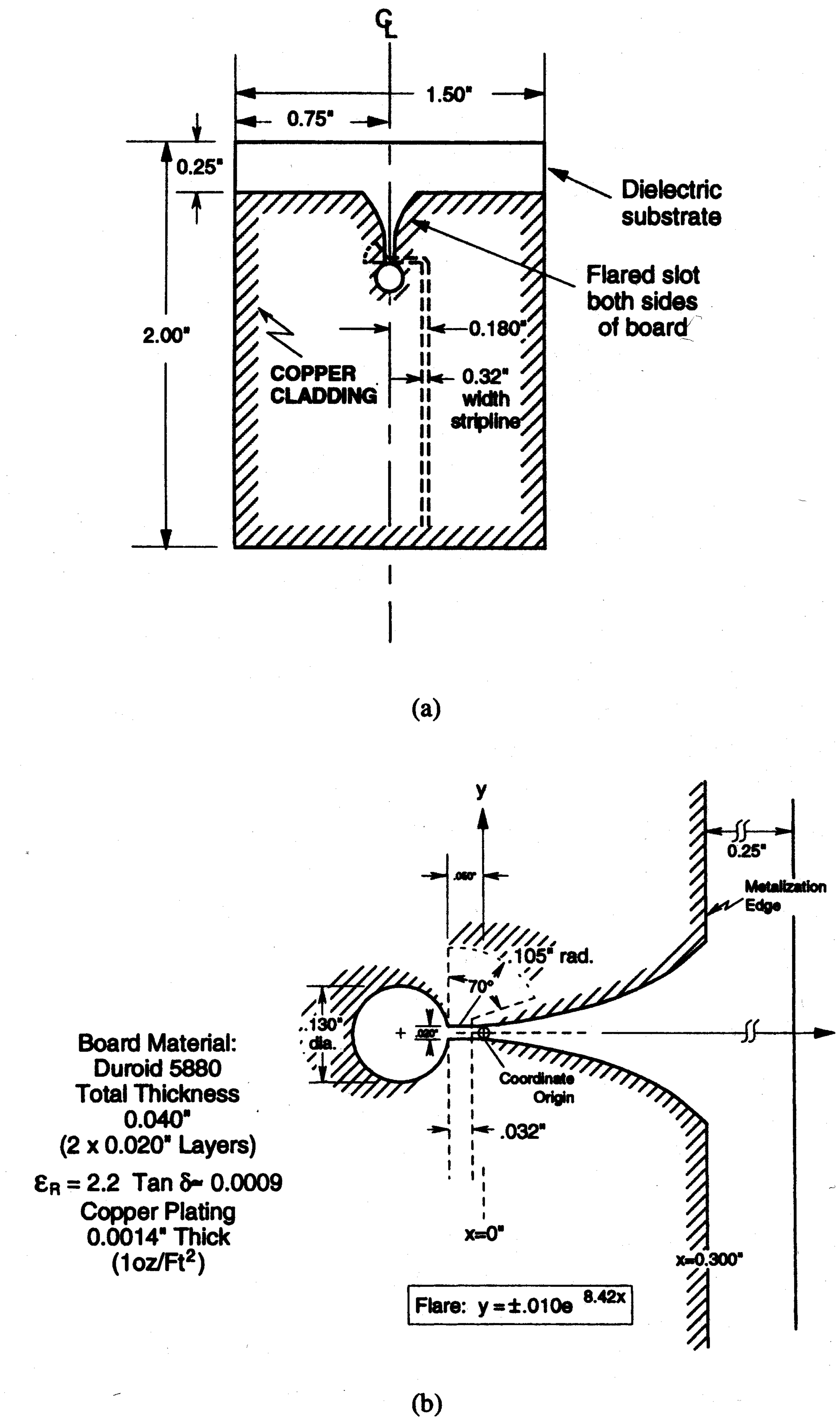

Fig. 1. Antenna geometry. (a) Vivaldi single-flare baseline element sketch; (b) Detail sketch of stripline feed and the slot element.

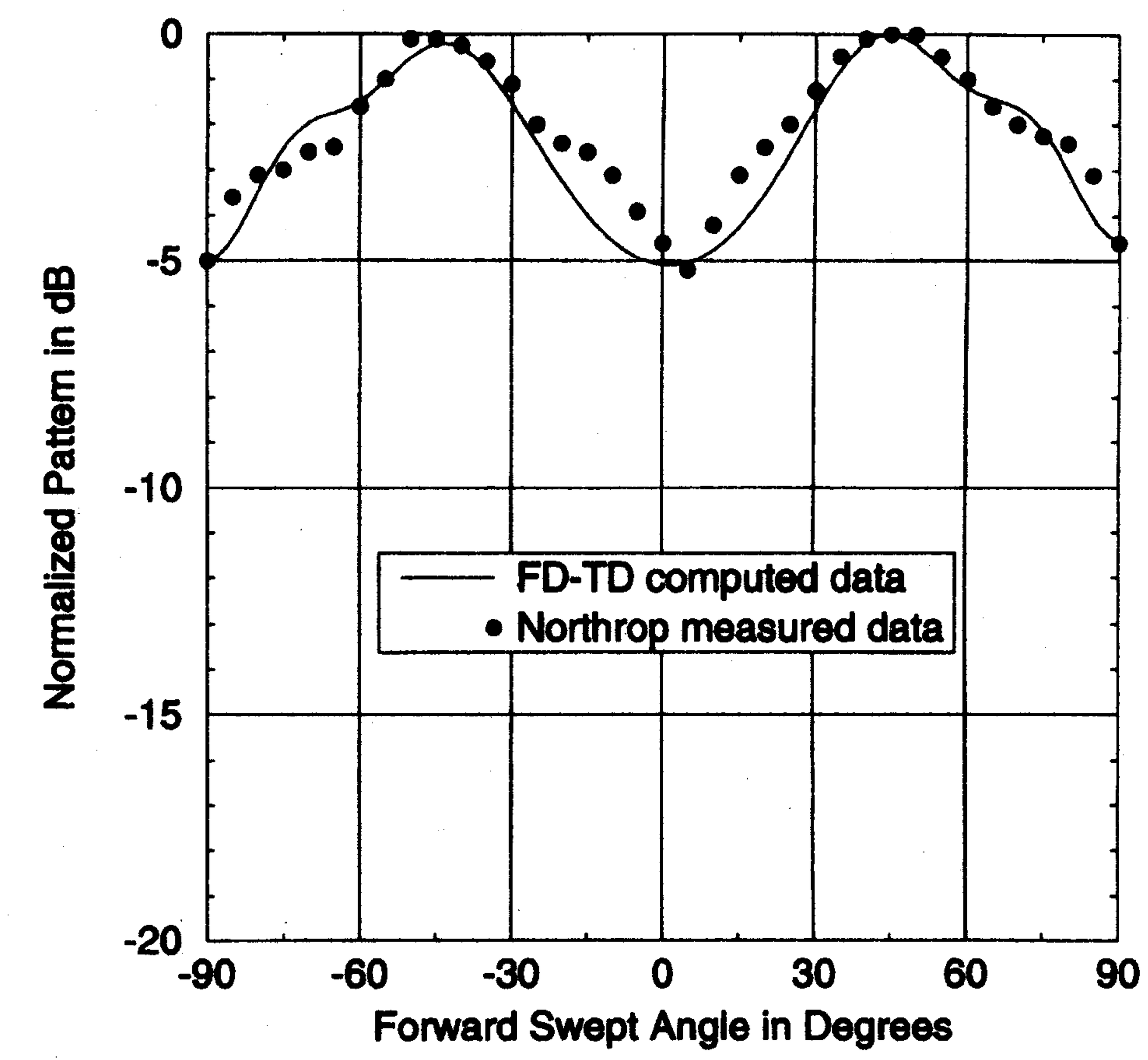

Fig. 2. Comparison of FD-TD computed and measured E-plane co-pol patterns. Baseline element at 12 GHz.

is capable of beam-steering and selectable polarization in either primary plane, and exhibits the characteristic broadband behavior of the Vivaldi. Preparatory to the study of this complex structure, we believed that it was important to study the cross-polarized radiation levels of a single Vivaldi. Due to the orthogonality of the crossed-pair sub-array element, the cross-pol of a single Vivaldi could significantly impact overall array performance. Mitigation of cross-pol radiation was therefore an important, but secondary, focus of early research.

A. Implementation

The baseline model consists of the geometry shown in Fig. 1. Initial FD-TD simulations involved excitation of this geometry at 6 GHz, 12 GHz, and 18 GHz. The resolution of the computational grid was based on the smallest physical dimension, namely, the throat of the horn. This dimension is 0.05 cm, and it corresponds to $\lambda_0/33$ at 18 GHz and $\lambda_0/99$ at 6 GHz. This high-resolution permitted the stepped-edge FD-TD model to simulate the radiation characteristics of the antenna nearly as accurately as a conformal surface FD-TD model that had been simultaneously developed. Thus, all subsequent modeling was done using stepped-edge FD-TD.

The examination of these problems with FD-TD is numerically intensive, requiring the use of supercomputers. All runs were completed on Cray Research supercomputers. With one exception, the grid size for all single-flare and double-flare Vivaldi problems was $42 \times 116 \times 142$ cells, corresponding to 4.15-million field unknowns. For single-flare and double-flare runs, CPU times for the Vivaldi antenna were on the order of 1100 s for a single-processor Cray-2 and 800 s for a single-processor Cray Y-MP.

B. Computed and Measured Results—Single Flare

The results shown here are for the baseline element given in Fig. 1. All patterns are angular sweeps in the plane of the horn (E-plane), with 0° being the forward radiation direction. Both co-polarized and cross-polarized radiation patterns were obtained. For the co-pol pattern, the E-field is measured in the E-plane of the antenna, while for the cross-pol pattern the E-field is measured perpendicular to this plane. In all co-pol/cross-pol plots presented, the co-pol has a greater magnitude than the cross-pol. For the baseline element, the co-pol radiation exceeds the cross-pol by about 50 dB in the forward region at 0°.

Consider first the FD-TD computed results for the co-pol radiation pattern of a single element at 12 GHz and the comparison with measurement (Fig. 2). FD-TD is seen to predict the ± 2.5 dB ripple in the main beam very well. This ripple appears to be a quite subtle feature of the pattern[1].

Measured data for the single-element Vivaldi indicate significant amounts of cross-polarized radiation. Measured levels of this radiation are on the order of -10 to -20 dB relative to

[1] In fact, test data for the baseline antenna indicated the ripple was present in the radiation pattern of the antenna when measured in one anechoic chamber, while the same antenna measured in another chamber gave no evidence of the ripple.

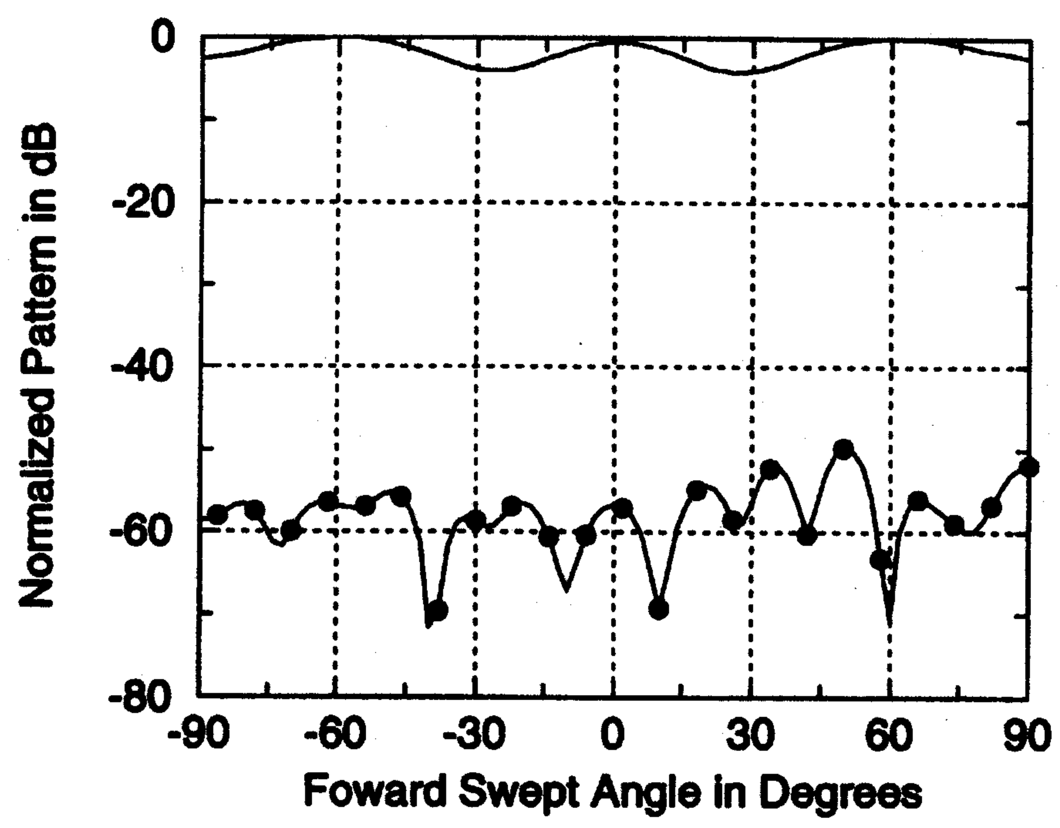

(a)

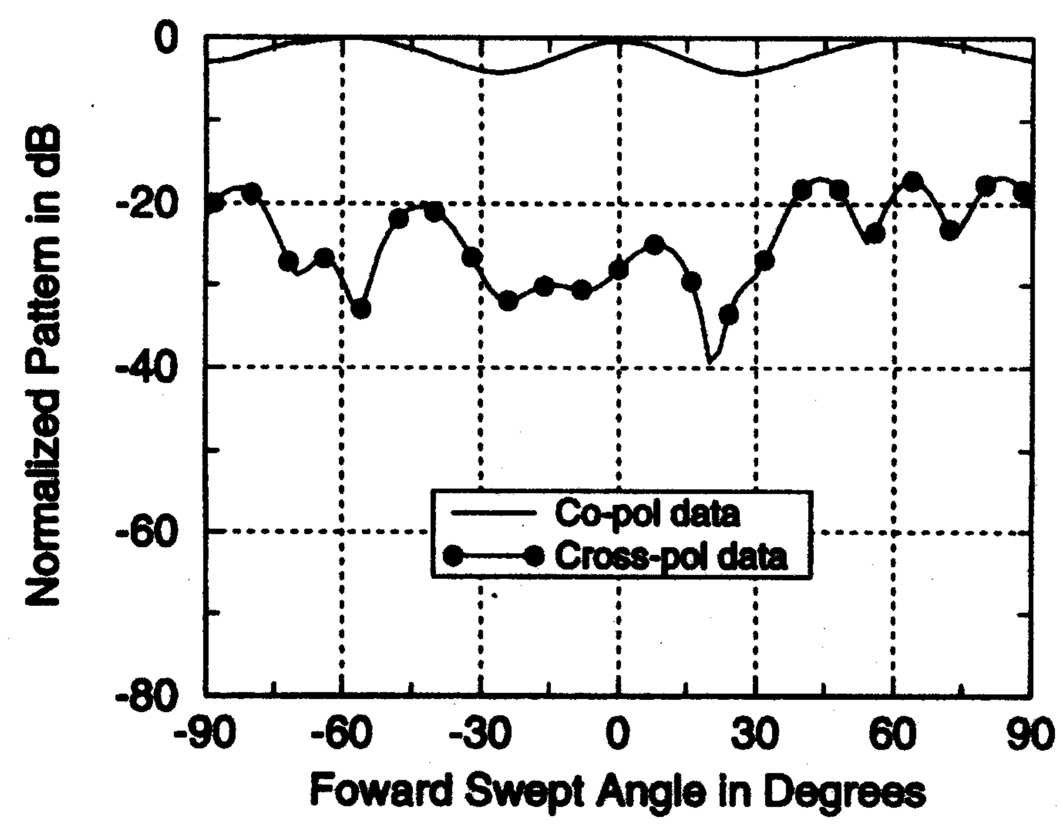

(b)

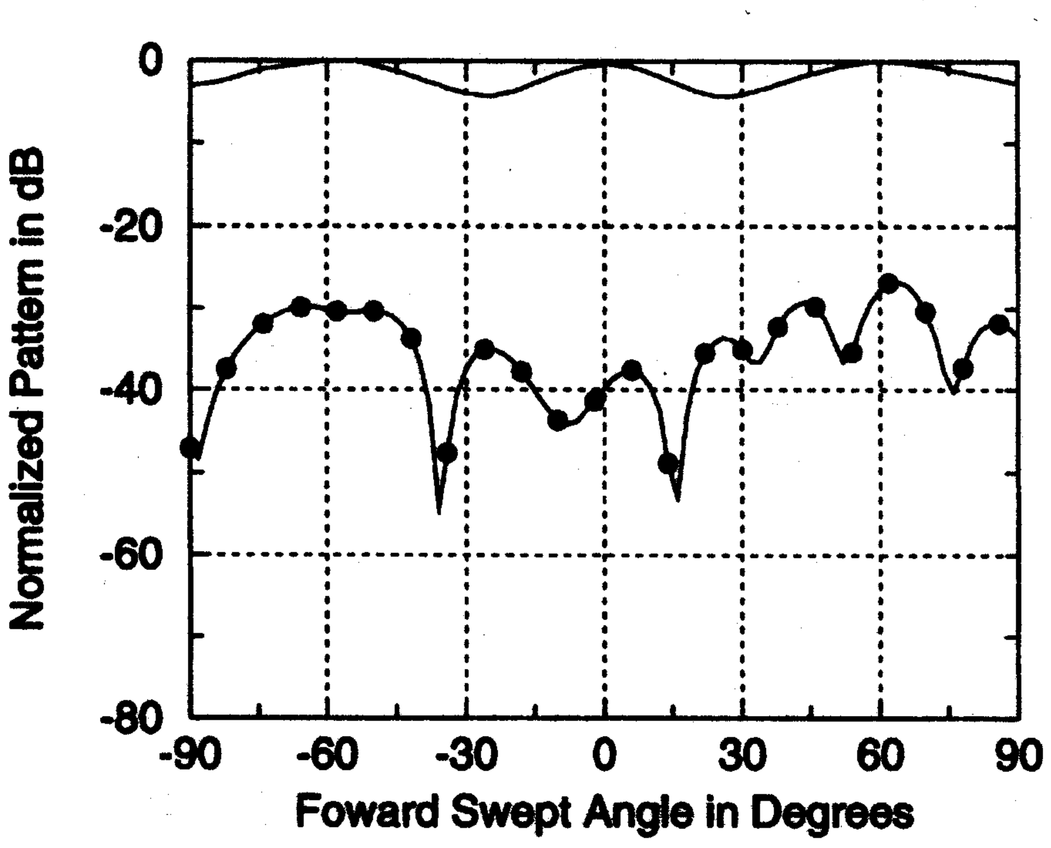

(c)

Fig. 3. FD-TD computed E-plane co-pol and cross-pol patterns at 18 GHz. (a) Baseline element; (b) baseline element, bottom ground plane shifted, asymmetrical feed; (c) baseline element, bottom ground plane shifted, asymmetrical feed, with grounding pins.

co-pol, and in some instances rise to the co-pol level. These cross-pol levels are much greater than those predicted by the FD-TD runs, approximately -50 dB. (For example, consider the results for the 18 GHz run shown in Fig. 3(a)). This can be explained by the fact that the computational model has a perfectly symmetrical geometry and source condition. From a physical standpoint, it could be argued that nothing exists in the FD-TD model to support the vertical currents necessary to give rise to cross-pol. The FD-TD results do show, however, that the design (not assembly) of the element itself exceeds the system requirements.

It was therefore sought to perturb the FD-TD model to qualitatively simulate possible construction artifacts of the test antenna due to the hand assembly of this element. The intent was to see if these artifacts could increase the order-of-magnitude of the computed cross-pol level (initially at -50 dB relative to computed co-pol) to approximate the measured cross-pol (at -10 dB to -20 dB). The first idea was to investigate a possible geometrical asymmetry of the stripline feed that might exist in the hand-assembled physical model. We simulated this by forcing the source to have an amplitude of 1 volt/cell above the stripline and 0.9 volts/cell below the stripline. At 6 GHz and 12 GHz, computed peak values of cross-pol rose to near -35 dB, and at 18 GHz they rose above -30 dB. It should be noted, however, that this did not change the co-pol pattern.

The second modification made to the baseline FD-TD model was to shift the bottom ground plane by one cell (0.5 mm) with respect to the top ground plane. This was motivated by the possible existence of misalignment due to hand assembly of the physical element. While this misalignment may be somewhat larger than what actually exists, the discretization of the grid did not allow for smaller changes. The results offer insight into the significance of a misalignment problem.

Fig. 3(b) shows the computed pattern at 18 GHz with an asymmetrically fed element and the bottom ground plane shifted. The predicted cross-pol is seen to rise dramatically to -20 dB at peak (forward region). Both of these model changes together brought the computed cross-pol to near the order of magnitude of the measured levels, i.e., -10 to -20 dB relative to the co-pol.

Due to the effect cross-pol radiation may have on the performance of this antenna in its context as an array element, we have investigated means to reduce it. Specifically, we verified empirical studies that suggested placing grounding pins between the upper and lower ground planes along the front edge and around the flare reduces the cross-pol.

A number of FD-TD runs were made to examine the impact of the grounding pins. Consider the run at 18 GHz, representing the worst-case cross-pol model (shifted bottom ground plane, asymmetrical feed), with grounding pins modeled in place. In Fig. 3(c), the computed cross-pol is seen to drop about 12 dB with respect to Fig. 3(b). This corresponds well with the observed order-of-magnitude cross-pol reduction seen in the measured data when grounding pins are present. It is also noted that the grounding pins in no way influence the computed co-pol pattern.

C. Computed and Measured Results—Double Flare

Fig. 4 gives the geometry for a two-element Vivaldi pair. Note that this model only differs from the baseline model in overall size, with the ground planes narrowed to 1 in and the dielectric along the front edge removed. The stripline feed and slot element geometries are the same as shown in Fig. 1(b). Empirical data suggested these changes helped improve performance.

Fig. 5 compares measured and FD-TD computed co-pol patterns at 12 GHz. Good-to-excellent agreement in the main beam is seen throughout the 180° range. It should be noted in this figure that the measured data were shifted because a beam shift, or squint, of approximately 7° was observed at 18 GHz. The probable physical basis for this squint is a phase

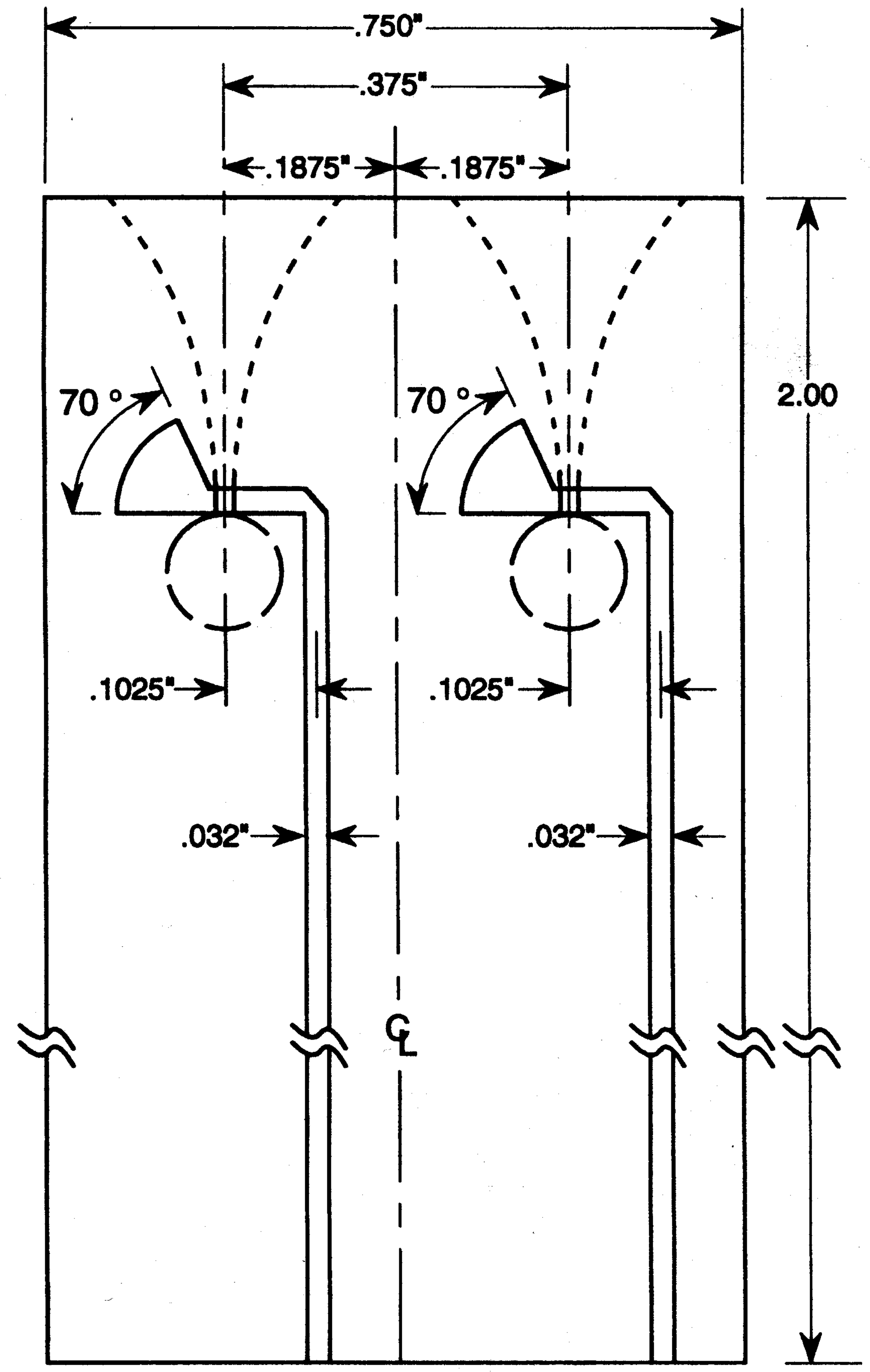

Fig. 4. Vivaldi double-flare geometry sketch.

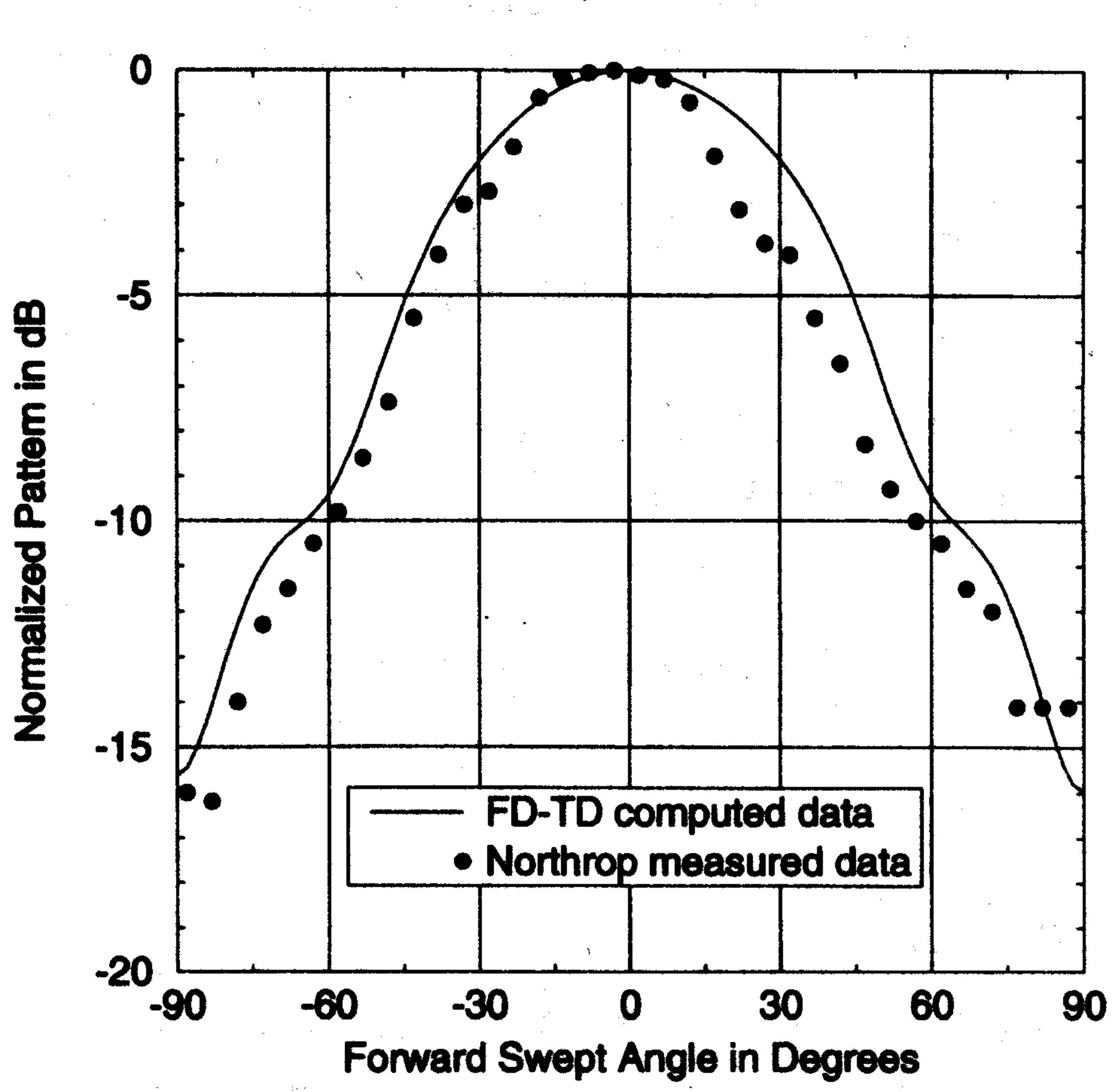

Fig. 5. Comparison of FD-TD computed and measured E-plane co-pol patterns. Double-flare at 12 GHz.

offset in the excitation of the elements. With the elements fed by two coaxial lines, it was determined by Northrop that a 10° beam squint could result from as little as a 0.045-in difference in line length.

D. Computed and Measured Results—LTSA Validation

To further validate the FD-TD model, we compared its predictions for radiation patterns of an LTSA to measured

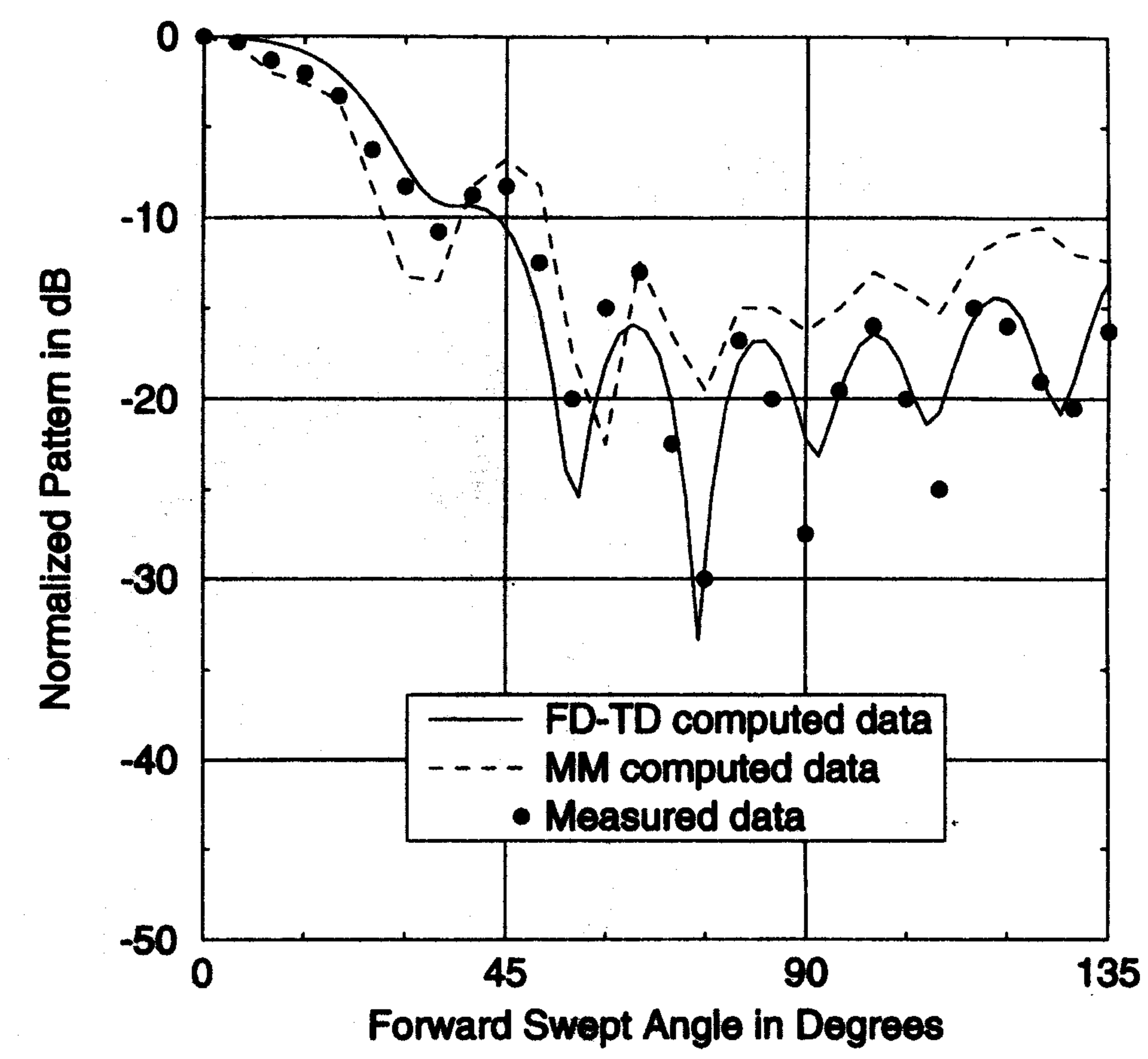

Fig. 6. Comparison of computed (FD-TD and MM) and measured E-plane co-pol patterns. LTSA validation model at 9 GHz.

and MM-computed patterns reported by Janaswamy [6]. The LTSA validation model from [6] had the following physical parameters: length, $L/\lambda_0 = 3.0$; ground plane width, $H/\lambda_0 = 0.9$; substrate thickness, $d/\lambda_0 = 0.021$; substrate permitivitty, $\epsilon_r = 2.33$; and flare angle, $2\alpha = 12.0°$. The frequency was 9 GHz, and FD-TD grid resolution was defined by the substrate thickness. The results can be seen in Fig. 6, which replicates Fig. 6 of [6] and adds our FD-TD results for comparison. Through the first 60° relative to forward, there is good agreement between the three data sets. Beyond 60°, the MM results provide a poorer level of agreement with measurements than the FD-TD model, predicting sidelobes that are as much as 6 dB to 10 dB above the measurements.

IV. Quad Element Results

A. Implementation

With the study of planar geometries for the Vivaldi completed, analysis of the sub-array element, or quad element, was the next task. The geometry for this problem is more complicated than for the planar element, consisting of two double flares (modeled in the previous section) perpendicular to each other, forming a "+" (Figure 7a).

The Cartesian nature of the FD-TD grid was well suited to examining the orthogonal array elements. The horizontal plane of the quad element was defined to be in the xy-plane, while the vertical plane was defined in the yz-plane. However, this arrangement caused the array axis to lie along a 45° line in the xz-plane. While creating no problems for the FD-TD time-stepping equations, it necessitated a change to the far-field computations. Since the array lies along a diagonal in the FD-TD grid, normal θ or ϕ pattern cuts are not possible, as both θ and ϕ are varying. To account for this, a great circle cut was made. This involved defining two rotated axes, x' and z', determining their unit vectors, and using these unit vectors to define a rotation matrix through which θ' and ϕ' could be mapped to the standard θ and ϕ spherical coordinates. This was able to provide an E-plane scan with respect to

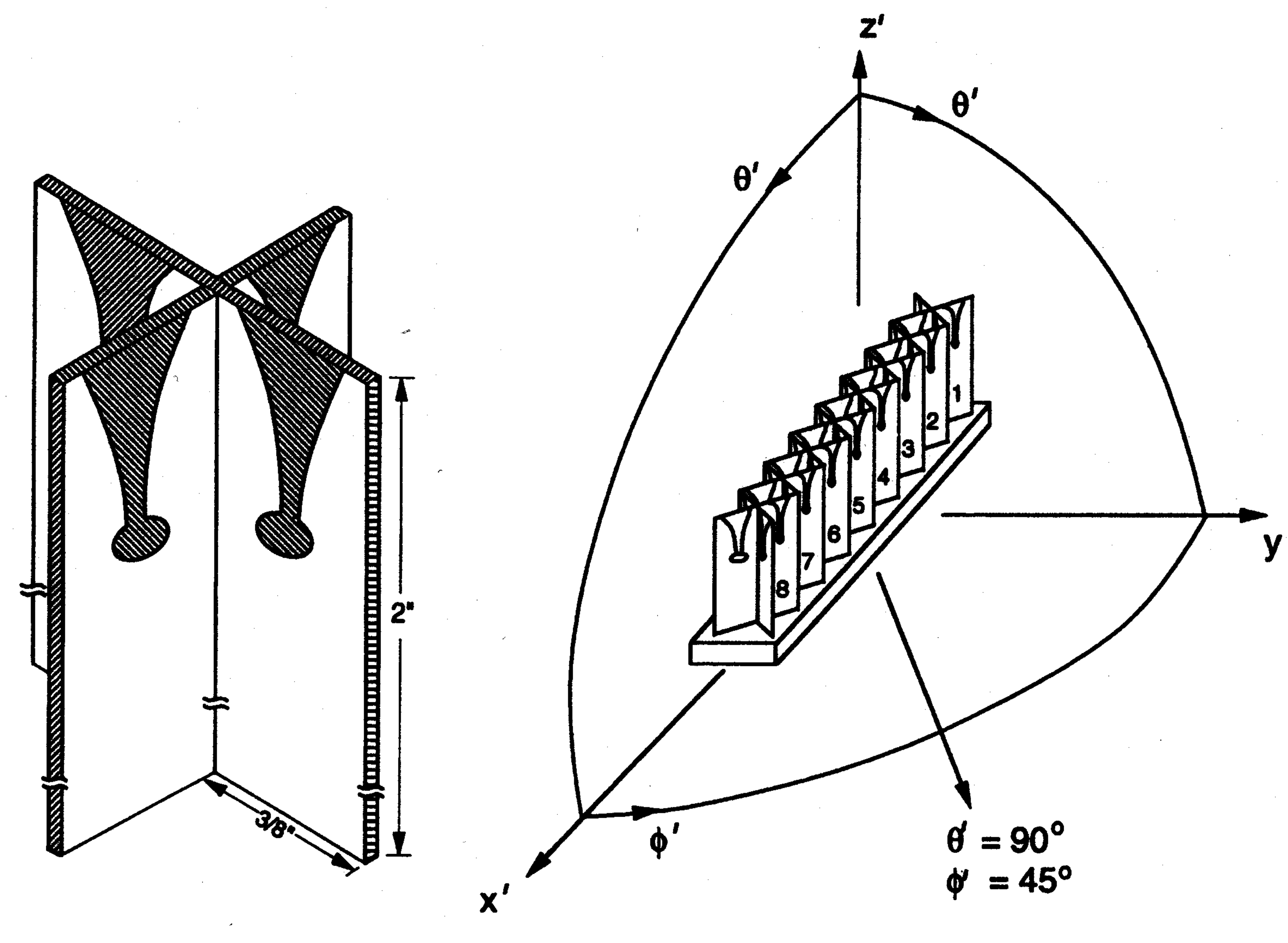

Fig. 7. Geometry sketches. (a) Single quad element; (b) eight-element array.

the diagonal orientation of the array. Furthermore, the far-field radiation components, E_θ and E_ϕ, were rotated to obtain the correct correspondence to co-pol and cross-pol radiation. These pattern cuts were used for both the single quad element and the eight-element array.

The FD-TD source used for this antenna generated single-frequency sinusoids. While a broadband pulse excitation would have been capable of covering the 6–18 GHz frequency band in one run (thereby saving computer resources), we elected to use single-frequency excitations. The justification for this is that time is discrete in the FD-TD solver. A time delay between pulses to effect the beam-steer may only be resolved to the discrete times $n\Delta T$. These discrete times translate to a discrete number of beam-steer angles, which may or may not correspond to the angles of interest. Single-frequency excitations allow for precise control of the phase taper along the length of the array, and thus precise control of the beam-steer angle. Pulse excitation of these antennas will be used in future impedance studies, and the extent of the error introduced by this discrete time delay will be examined.

For the single quad element, a grid size of $82 \times 82 \times 140$ was used, requiring solution of 5.65-million vector field unknowns. Run times were on the order of 1600 s using a single-processor Cray YMP-8.

B. Computed and Measured Results

Comparisons between FD-TD computed data and measured data were favorable for the quad element. Consider the results for 18 GHz shown in Fig. 8. Good-to-excellent agreement is seen over $\pm 70°$. While FD-TD predicts a symmetric pattern, measured data are not symmetric. In particular, the measurements confirm the presence of a "shoulder" at $-40°$. Furthermore, the first sidelobes at $\pm 70°$ are tracked, but the measured levels differ by about 7 dB. In fact, the first sidelobes in the FD-TD pattern appear to be the geometric mean of the asymmetrical measured sidelobes.

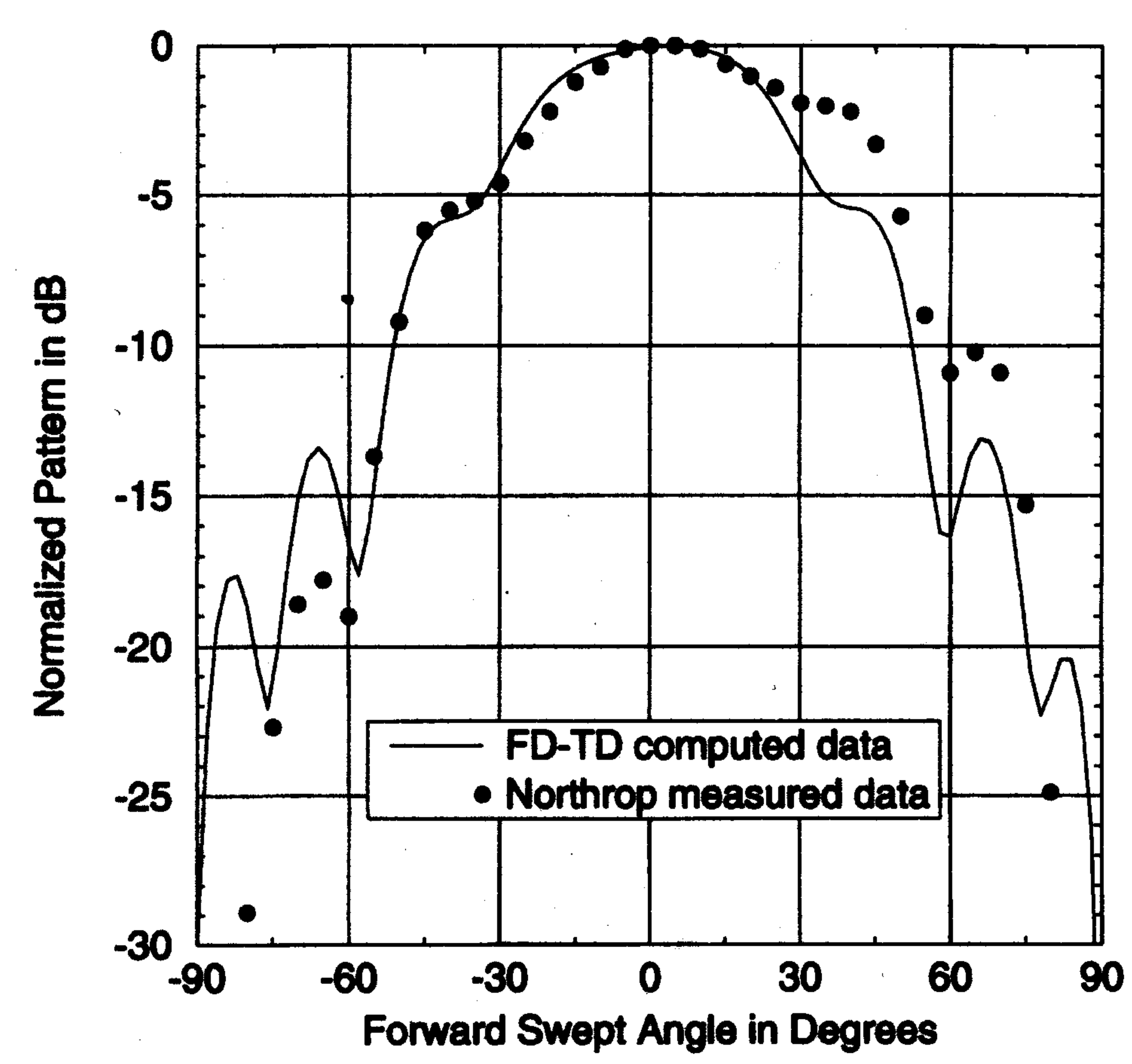

Fig. 8. Comparison of FD-TD computed and measured E-plane co-pol patterns. Single-quad element at 18 GHz.

V. Array Results

A. Implementation

In this section, we report FD-TD results for an eight-element array of Vivaldi quads sketched in Fig. 7(b). This is a linear array, and it can be excited with varying phase and amplitude distributions to permit beam-steering and polarization selection. Overall, we computed co-pol and cross-pol gain patterns in the plane of the array (E-plane) for frequencies of 6, 9, 12, 15, and 18 GHz. However, only the results for 18 GHz are presented here, as this frequency best demonstrates the development of the grating lobe. Using appropriate phase distributions at these frequencies, we implemented beam-steer angles of 0°, 20°, 45°, and 60° (see Fig. 9). This was achieved by simply incorporating the proper phase shift in the sinusoidal excitation of the stripline feed. Determination of the phasing β for beam-steer is obtained from $\beta = kd \sin\theta$, where the

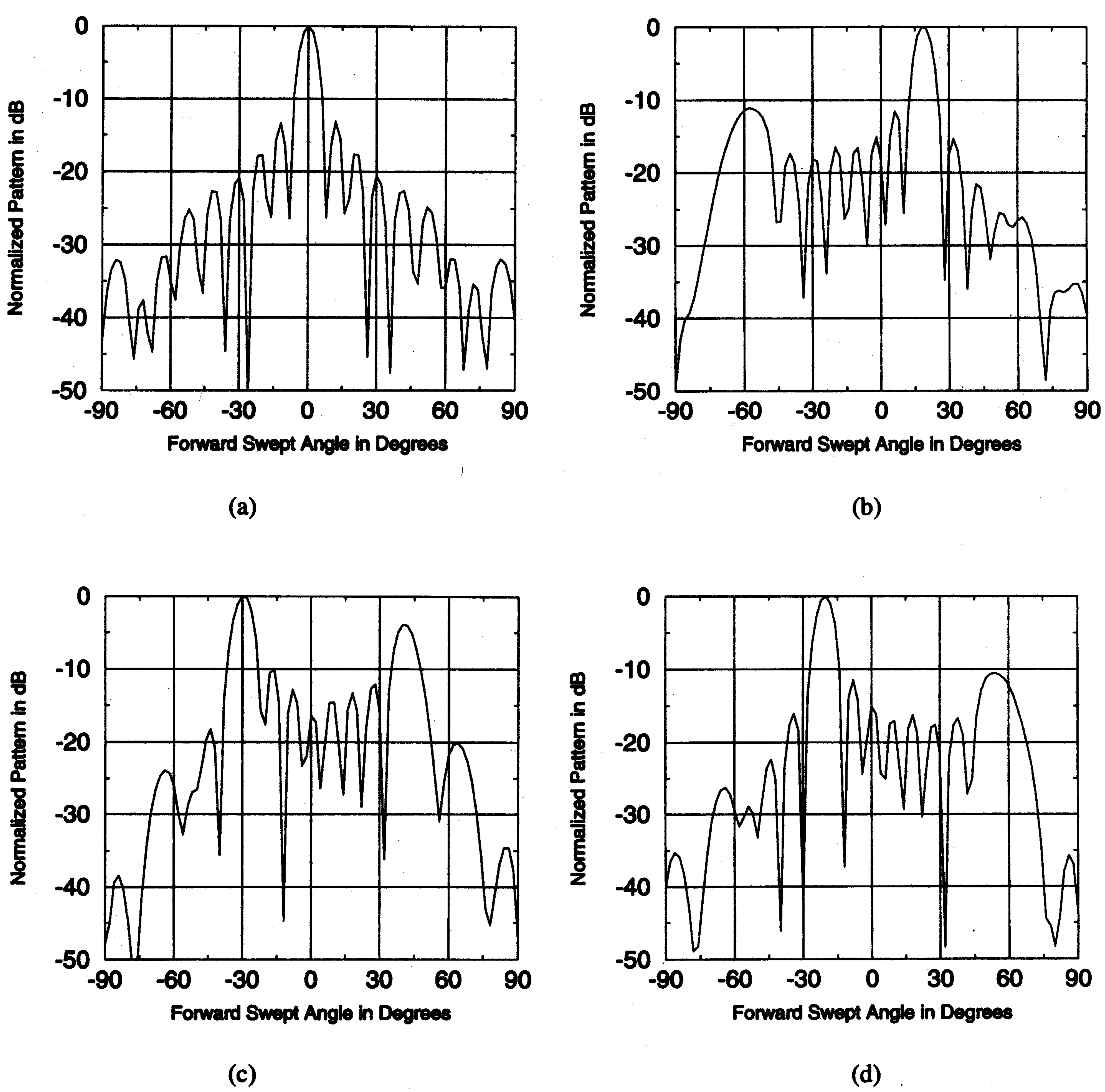

Fig. 9. FD-TD computed E-plane co-pol patterns. Eight-element array at 18 GHz. (a) No beam steer; (b) 20° beam steer; (c) 45° beam steer; (d) 60° beam steer.

wavenumber $k = 2\pi/\lambda_0$, the element spacing $d = 0.53$ in, and θ is the desired beam-steer angle.

The eight element array increased the grid size to 222 × 222 × 140. The number of vector field unknowns solved for was 41.4 million. Run times were on the order of one CPU hour using automatic multiprocessor tasking on a dedicated Cray YMP-8.

B. Computed and Measured Results

For the case of endfire (no beam-steer), the eight-element array produces a narrower main beam and lower sidelobe levels than the single quad element, as expected. For all frequencies examined, the expected $\sin x/x$ pattern predicted by array theory is seen, with more oscillations occurring as frequency is increased due to the greater number of wavelengths along the length of the array.

At 18 GHz (Fig. 9(a)), the FD-TD computed main beam for the array is much more narrow than that of the single quad element, and has sidelobe levels near -13 dB. The results for a beam-steer angle of 20° can be examined in Fig. 9(b). Here, the main beam has narrowed further and the sidelobe levels are about the same. However, a grating lobe is also seen in this figure. In Fig. 9(c), the beam-steer angle was increased to 45°. Here the grating lobe has increased to 4 dB relative to the main beam, with the first sidelobe level at -9 dB and the sidelobes rise as the grating lobe is approached. Finally, in Fig. 9(d), the case of 60° beam-steer was examined. Here the grating lobe dominates the pattern, rising to 11 dB relative to the main beam. The first sidelobe is only at -6 dB down, again increasing towards the grating lobe.

As shown in Fig. 10(a), excellent agreement between FD-TD and measured data is obtained for a beam-steer angle of 0° at 6 GHz. The main beam width is matched, as are sidelobe levels. The measured data appear to have a slight asymmetry. In Fig. 10(b), at 12 GHz, very good correspondence is seen for a beam-steer angle of 45°. The main beam is very accurately tracked, as are sidelobes. The first, fifth, and sixth measured nulls are somewhat deeper than the predicted levels. Correspondence is maintained over 100° of the region off the main beam.

Simple array theory can be used to qualitatively predict the results seen in this section. We note that in both the computed and measured patterns, the beam-steer angle is not quite reached. For example, choosing a desired beam-steer angle of 60° results in an *actual* beam-steer angle of approximately 55° (Fig. 9(d)). Array theory predicts the overall radiation pattern to be the product of the element pattern and the array factor. The deviation of the beam steer angle is attributable to this pattern multiplication. Array theory can also be used to predict one of the most notable features of these results, grating lobes. For a linear array, grating lobes will appear for element-to-element spacings of $d/\lambda_0 \geq 1/2$. The element

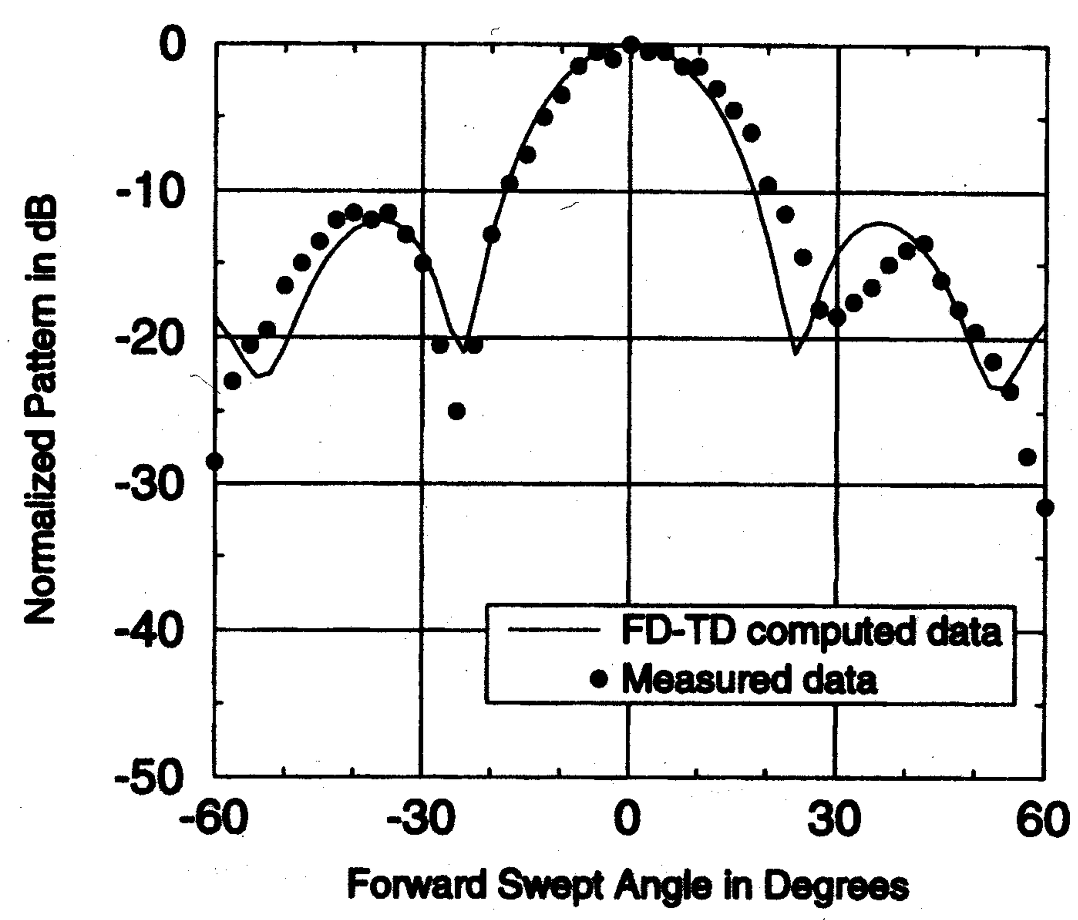

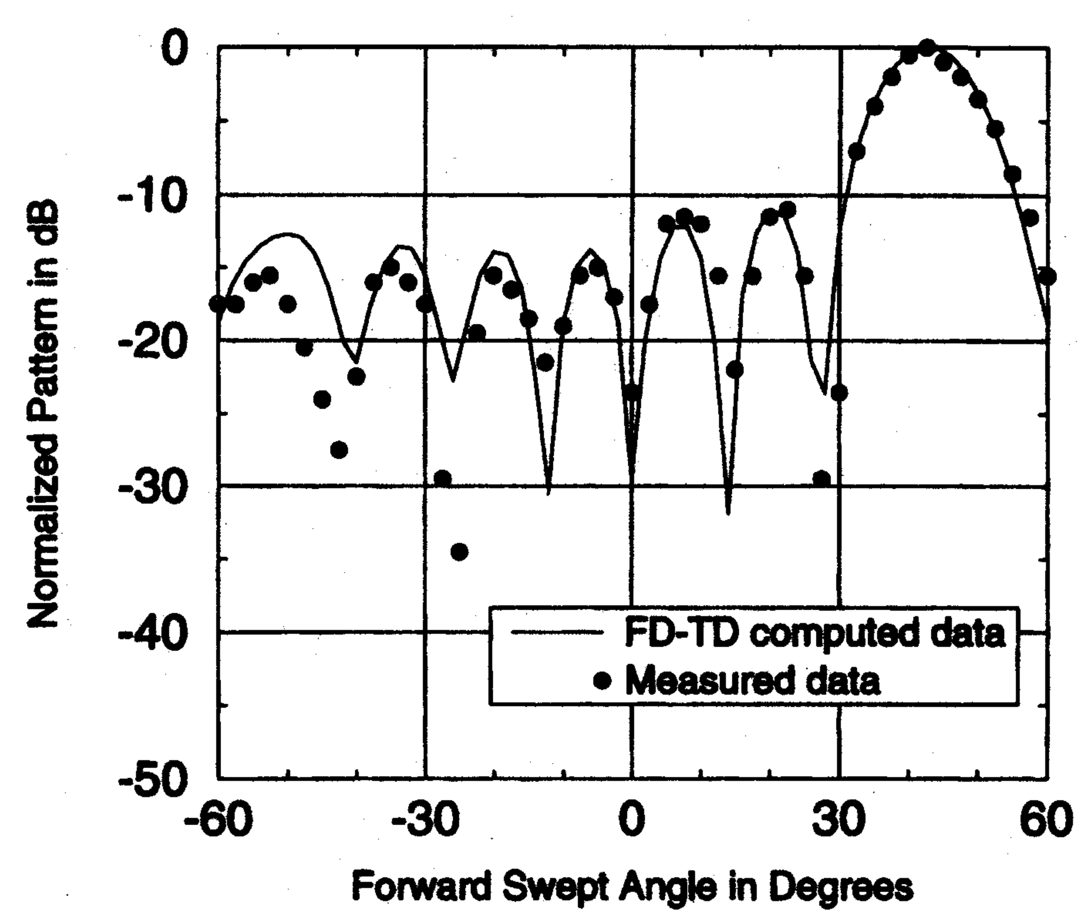

Fig. 10. Comparison of FD-TD computed and measured E-plane co-pol patterns. (a) Eight-element array at 6 GHz, no beam steer; (b) eight-element array at 12 GHz, 45° beam steer.

spacing, $d = 0.53$ in, gives rise to grating lobes at frequencies above 11.1 Ghz. Beginning at 12 GHz, grating lobes are seen in the FD-TD computed results. Furthermore, a simple array calculation shows the grating lobes to be almost exactly where they appear in the FD-TD results. The FD-TD prediction of these dominant features lends additional confidence to the results.

VI. Summary and Conclusion

Using the FD-TD technique to model radiation by tapered slot antennas, good-to-excellent agreement between computed and measured data has been obtained for single-flare and double-flare planar elements. For single-flare Vivaldis, subtle ripples in the co-pol pattern are observed in both the computed and measured patterns. The FD-TD studies for these antennas also demonstrated a large sensitivity of the cross-pol fields to slight alignment errors and feed asymmetries due to nonmachine construction of the antenna. Both FD-TD and measurements showed a similar level of reduction of cross-pol radiation when grounding pins are used to short the ground planes. Interestingly, the co-pol pattern exhibited no distortion with respect to the baseline model for any changes.

During the second phase of this work, we developed FD-TD models of a single quad element consisting of two orthogonal double-flare antennas. The quad element had the anticipated behavior. That is, with the antenna radiating in two planes, cross-pol levels rose compared to the levels seen with the planar element. Comparison with measurement was very good for the quad element.

Finally, we modeled a linear phased array comprised of eight quad elements. As expected, we computed main beam sharpening as the frequency and/or the number of elements increased. Further, as expected, we found that more elements created more sidelobes. The cross-pol levels may also present a problem for this array. Acceptable levels of cross-pol radiation must be determined by system requirements. Comparisons with measured data for the array showed some very good agreement, and anticipated qualitative trends in terms of both sidelobe and grating lobe locations and magnitudes were seen for the cases presented.

Acknowledgment

The authors thank D. Thompson and M. Radich of Northrop Corporation, Electronic Systems Division, Rolling Meadows, IL, for their contributions, including measurement data and design suggestions. Thanks are also extended to J. Ahnert and E. Harrigan of Cray Research, Inc., for providing the computational resources for this project. Finally, we thank M. Piket-May, formerly at Northwestern University (now at the University of Colorado at Boulder), for her assistance throughout this project.

References

[1] P. J. Gibson, "The Vivaldi aerial," in *Proc. 9th European Microwave Conf.*, pp. 101–105, 1979.
[2] S. N. Prasad and S. Mahapatra, "A new mic slot-line aerial," *IEEE Trans. Antennas Propagat.*, vol. AP-31, no. 3, pp. 525–527, May 1983.
[3] K. S. Yngvesson *et al.*, "Endfire tapered slot antennas on dielectric substrates," *IEEE Trans. Antennas Propagat.*, vol. AP-33, no. 12, pp. 1392–1400, Dec. 1985.
[4] R. Janaswamy, D. H. Schaubert and D. M. Pozar, "Analysis of the transverse electromagnetic mode linearly tapered slot antenna," *Radio Sci.*, vol. 21, no. 5, pp. 797–804, Sept.–Oct. 1986.
[5] R. Janaswamy and D. H. Schaubert, "Analysis of the tapered slot antenna," *IEEE Trans. Antennas Propagat.*, vol. AP-33, no. 9, pp. 1058–1064, Sept. 1987.
[6] R. Janaswamy, "An accurate moment method model for the tapered slot antenna," *IEEE Trans. Antennas Propagat.* vol. 37, no. 12, pp. 1523–1528, Dec. 1989.
[7] P. S. Simon, K. McInturff, D. L. Johnson, and J. A. Troychak, "Moment method analysis of a stripline-fed finite slot using subdomain basis function," in *Proc. 1989 Antenna Applications Symp.*, Univ. of Illinois, Sept. 1989.
[8] K. S. Yee, "Numerical solution of initial boundary value problems involving Maxwell's equations in isotropic media," *IEEE Trans. Antennas Propagat.*, vol. AP-14, pp. 302–307, May 1966.
[9] A. Taflove and M. E. Brodwin, "Numerical solution of steady-state electromagnetic scattering problems using the time-dependent Maxwells equations," *IEEE Trans. on Microwave Theory Tech.*, vol. MTT-23, pp. 623–630, Aug. 1975.
[10] B. Engquist and A. Majda. "Absorbing boundary conditions for the numerical simulation of waves," *Math. Comput.*, vol. 31, pp. 629–651, 1977.
[11] G. Mur, "Absorbing boundary conditions for the numerical simulation of waves," *IEEE Trans. Electromagn. Compat.*, vol. EMC-23, pp. 377–382, Nov. 1981.
[12] A. Taflove and K. Umashankar, "Radar cross section of general three-dimensional scatterers," *IEEE Trans. Electromagn. Compat.*, vol. EMC-25, pp. 433–440, Nov. 1983.

[13] A. Taflove, K. R. Umashankar, and T. G. Jurgens, "Validation of FD-TD modeling of the radar cross section of three-dimensional scatterers," *IEEE Trans. Antennas Propagat.*, vol. AP-33, pp. 662–666, June 1985.
[14] T. Jurgens, A. Taflove, K. Umashankar, and T. Moore, "Finite difference time domain modeling of curved surfaces," *IEEE Trans. Antennas Propagat.*, vol. 40, no. 4, pp. 357–366, Apr. 1992.

Eric Thiele (S'86) was born in Columbus, OH, on July 14, 1965. He received the B.S.E.E. degree from the University of Dayton, Dayton, OH, in 1988, and the M.S. and Ph.D. degrees in electrical engineering from Northwestern University, Evanston, IL, in 1990 and 1994, respectively.

While attending the University of Dayton, he co-oped as an Engineering Assistant at Mission Research Corp. in Dayton. His primary work there involved the examination of a number of different EM scattering problems. After graduating in 1988, he worked for MRJ, Inc., Oakton, VA, until September of 1989 as a Member of the Technical Staff. His work there focused on software development for different EM numerical tools on the massively parallel Thinking Machines Corp. Connection Machine. His research interests include computational modeling of electromagnetic interaction and propagation problems, with an emphasis on antennas, antenna arrays, and scattering.

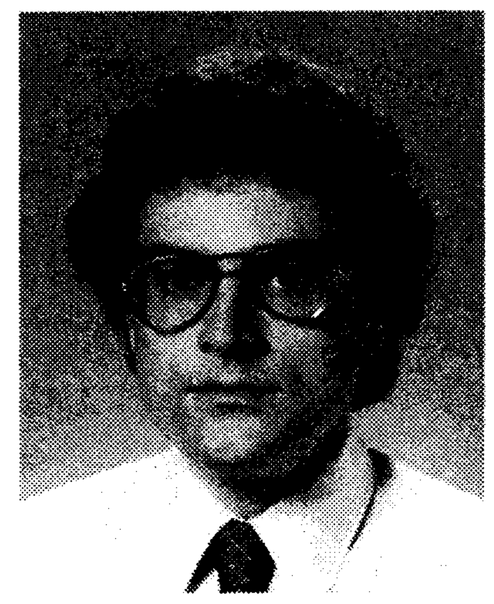

Allen Taflove (F'90) is a Professor in the Department of Electrical Engineering and Computer Science, McCormick School of Engineering, Northwestern University, Evanston, IL. His current research interests include first-principles Maxwell's equations supercomputing simulation of nanosecond-regime electronic circuits and subpicosecond-regime nonlinear optical phenomena and devices.

Dr. Taflove was named an IEEE Fellow for "contributions to the development of the finite-difference time-domain (FD-TD) solution of Maxwell's equations." Since the end of 1989, he has given 50 invited talks and lectures in the U.S. on horizons in supercomputing computational electromagnetics. In 1990–91 he was a Distinguished National Lecturer for the IEEE Antennas and Propagation Society, and in 1992 he was Chairman of the Technical Program of the IEEE Antennas and Propagation Society International Symposium, Chicago, IL. He originated several innovative programs in the McCormick School, including the Honors Program in Undergraduate Research (a seven-year combined B.S./Ph.D. engineering degree program for extremely talented students), the Undergraduate Design Competition, and the High School Outreach Program. In 1991, he was named McCormick Faculty Adviser of the Year. He is a member of Eta Kappa Nu, Tau Beta Pi, Sigma Xi, the International Union of Radio Science (URSI) Commissions B and K, the Electromagnetics Academy, AAAS, and the New York Academy of Sciences. His biographical listings include *Who's Who in Engineering*, *Who's Who in America*, *Who's Who in Science and Engineering*, and *Who's Who in American Education*.